

Supporting Information

***In-situ* controlled synthesis of porous Fe-N-C materials from oily sludge by chlorinating calcination and their novel application in supercapacitors**

Hanfeng Zhou^{a,c}, Zhibo Deng^a, Tianbao Liu^a, Tao liu^{a,c}, Lijuan Zhang^{a}, Xintai Su^{a,b,c}, Zhang Lin^{a,b,c}*

^a School of Environment and Energy, Guangdong Provincial Key Laboratory of Solid Wastes Pollution Control and Recycling, South China University of Technology, Guangzhou, Guangdong 510006, China.

^b Guangdong Engineering and Technology Research Center for Environmental Nanomaterials, Guangzhou 510006, PR China.

^c Sino-Singapore International Joint Research Institute (SSIJRI), Guangzhou 510000, China.

* Corresponding author: zhanglj@scut.edu.cn and zhanglj@scut.edu.cn

Part S1 Experimental section

Electrochemical measurement. Supercapacitor electrochemical properties of FNC-500, NC-600, and NC-400 were performed on a three-electrode system in an aqueous KOH electrolyte (6.0 M), in which a platinum wire served as the counter electrode and an Hg/HgO electrode was used as the reference electrode. The working electrode was fabricated as follows: 8 mg of as-prepared products were mixed with 1 mg of acetylene black and 165 μL of polytetrafluoroethylene (PTFE) emulsion at a weight ratio of 8: 1: 1 with the addition of 5 mL of ethanol. The mixture was then evenly dispersed via an ultrasonic device. Subsequently, the dispersed mixture was coated to a 3 cm^2 nickel foam (the mass load: 0.0032g). Before the electrochemical measurement, the working electrode was pressed to film and soaked in 6.0 M KOH for 12 h. Cyclic voltammetry (CV) was measured in the potential range of -1.0-0 V from 0.005 to 0.1 $\text{V}\cdot\text{s}^{-1}$ for the scan rate. And the chronopotentiometry (CP) was measured at 0.5-10 $\text{A}\cdot\text{g}^{-1}$ over the same potential range. The A.C. impedance test was completed under a sweeping frequency ranging from 0.01 Hz to 10 kHz. All the measurements were finished under room temperature via an electrochemical workstation (CHI 660e, Shanghai Chen hua Instrument Co. Ltd., China).

The specific capacitance (C , $\text{F}\cdot\text{g}^{-1}$) of electrodes was calculated by GCD curves according to following equation:

$$C_m = \frac{I \cdot \Delta t}{m \cdot \Delta V} \quad (\text{S1})$$

where C_{m3} ($F \cdot g^{-1}$) is the specific capacitance in three electrode system and C_{m2} ($F \cdot g^{-1}$) is the specific capacitance in two electrode system, I (A) is the current, m (g) is the mass of electroactive materials, ΔV (v) is the voltage range, and Δt (s) is the discharge time.

The two symmetrical electrodes were separated using a polypropylene separator soaked with 6 M KOH electrolytes in a CR2032 stainless steel coin cell. The cyclic voltammetry and galvanostatic charge-discharge tests for these devices were performed in the potential range of 0-1.2V. Electrochemical impedance spectroscopy (EIS) was also performed in the frequency range of 10 kHz to 0.01 Hz at the open circuit voltage with an alternate current amplitude of 5 mV. The gravimetric capacitance for the single electrode was calculated according to eq 2:

$$C_m = \frac{4I \cdot \Delta t}{m \cdot \Delta v} \quad (S2)$$

Where, I (A) is the constant discharging current, ΔV (V) is the potential change within the discharge time Δt (s), and m (g) is the total mass of the active materials in the two electrodes.

The energy density (E_t , $Wh \cdot kg^{-1}$) and power density (P_t , $W \cdot kg^{-1}$) of symmetrical supercapacitor systems were calculated from the following equation:

$$E_t = \frac{1}{2} C_t (\Delta V)^2 \quad (S3)$$

$$P_t = \frac{E_t}{t} \quad (S4)$$

Where, C_t ($F \cdot g^{-1}$) is the specific capacitance of the total symmetrical system, ΔV (V) is the cell voltage for charging and discharging, and t (h) is the discharge time, respectively.

Part S2 Characteristic analysis of the original oily sludge

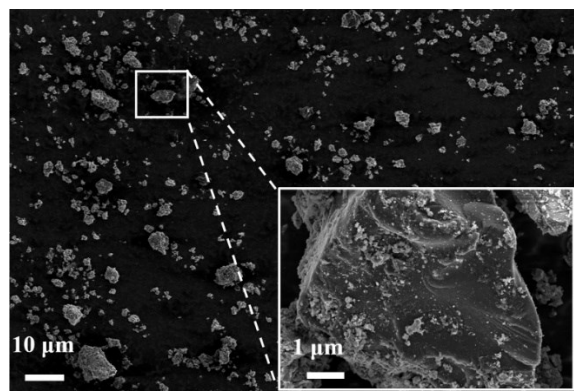


Figure S1. SEM image of the original oily sludge.

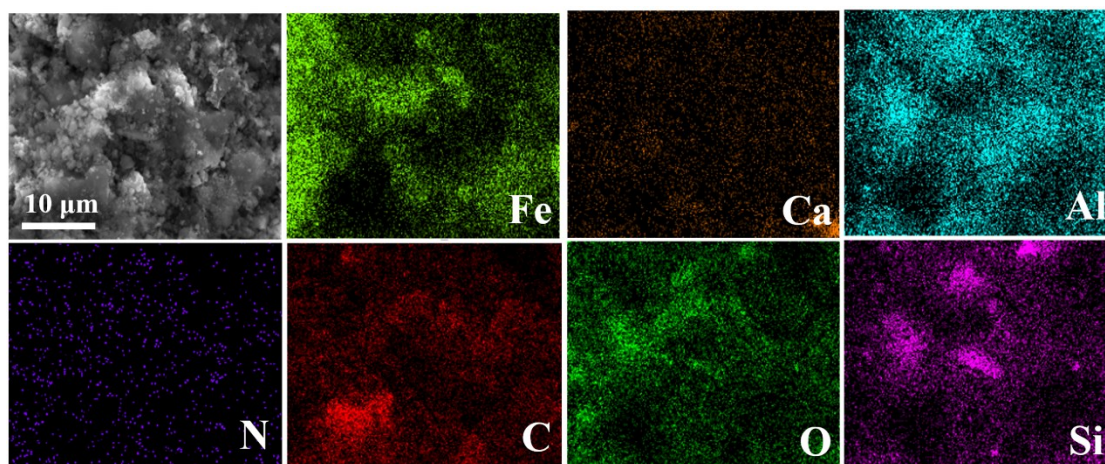


Figure S2. The corresponding EDS elemental mappings of the original oily sludge.

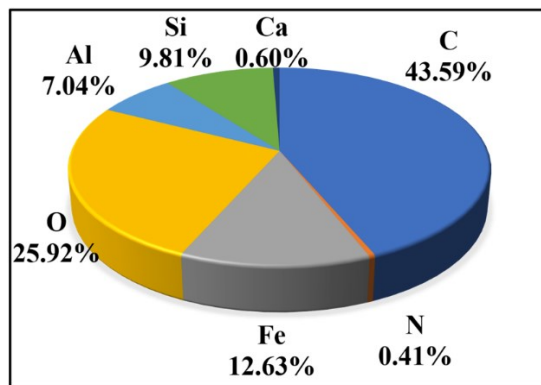


Figure S3. The distribution total number spectrum of EDS of the original oily sludge, and the proportion of different elements is the wt.%.

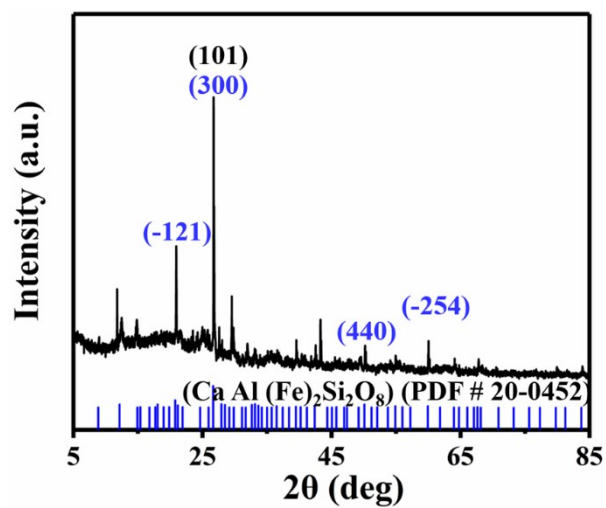


Figure S4. The XRD of the original oily sludge.

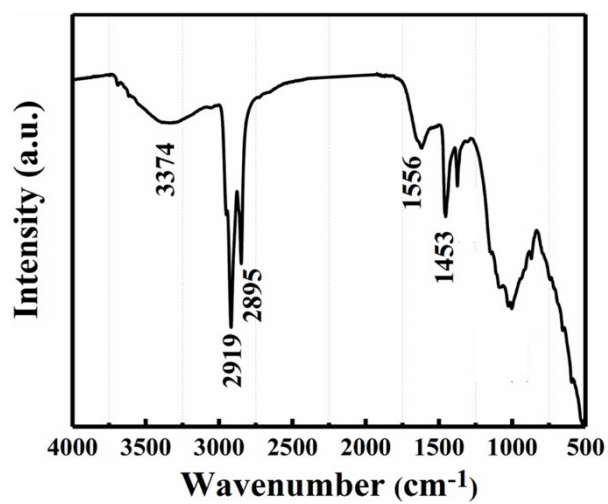


Figure S5. FT-IR of the original oily sludge.

Part S3 Preparation and characterization of porous Fe-N-C materials

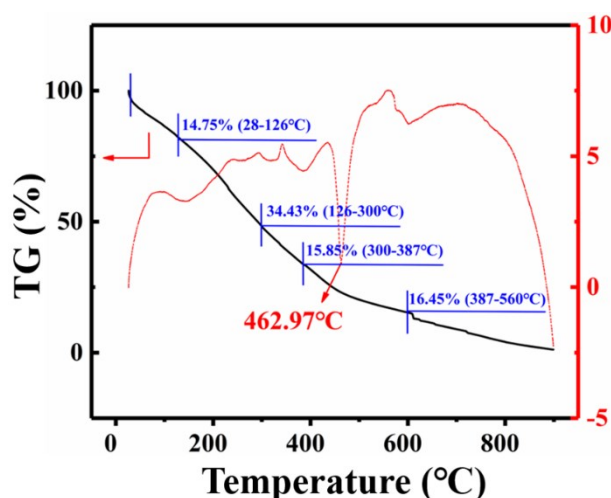


Figure S6. TG-DSC curves of the original oily sludge.

Specifically, it is observed from **Figure S6** that the TG curve of oily sludge shows a process of mass loss step by step. These steps include the loss of water (28-126 °C around 14.95 %), the decomposition of residual oil (126-300 °C, around 34.43 %), organic matter condensation (300-387 °C, around 15.85%), and inorganic phase decomposition (387-560 °C, around 16.45%), followed the carbonization of the sample (300-560 °C). As observed from DSC curve in **Figure S6** (red line), accompanied by the appearance of well-resolved endothermic signals centered at 340 and 560 °C, respectively. One of the very distinct exothermic peaks at 462.97 °C could be attributed to the decomposition of anorthite. Based on this, we can deduce that there is an exothermic peak at 462.97 °C in the DSC curve, which can be considered as an important turning point of some special phase transformation.

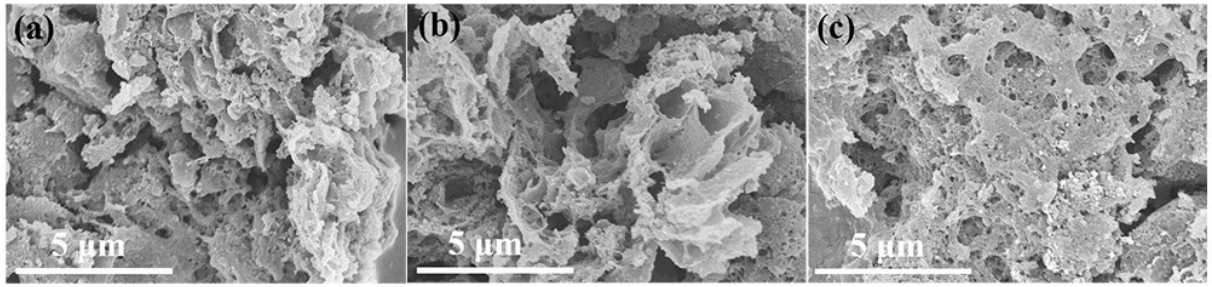


Figure S7. SEM image of NC-400 (a), FNC-500 (b) and NC-600 (c), respectively.

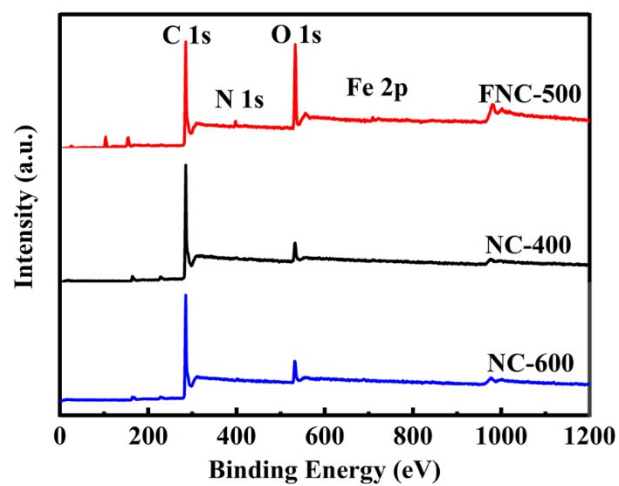


Figure S8. XPS survey spectra of NC-400, FNC-500 and NC-600, respectively.

Table S1. Elemental content of as-prepared samples calculated from the XPS survey spectra.

Sample	C (at. %)	O (at. %)	N (at. %)	Fe (at. %)
NC-400	93.79	2.34	1.34	0
FNC-500	86.92	8.92	3.12	0.27
NC-600	93.27	3.13	1.29	0

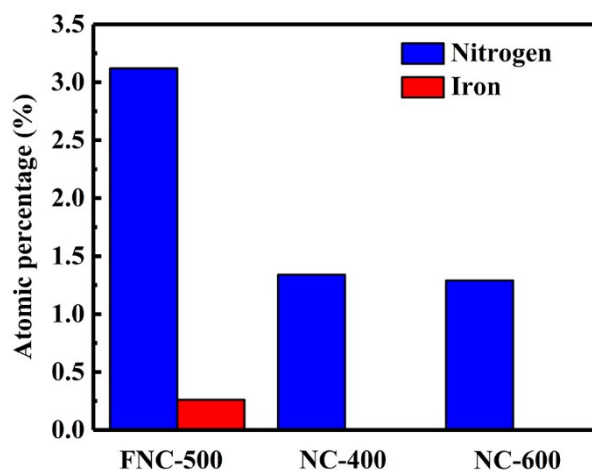


Figure S9. Iron and nitrogen content of NC-400, FNC-500 and NC-600 determined by XPS measurements.

Table S2 XPS atomic percentage of different types of N in FNC-500, NC-600, and NC-400.

Sample	Pyridinic-N (at. %)	Fe-N (at. %)	Pyrrolic-N (at. %)	Graphitic-N (at. %)	Oxidized-N (at. %)
NC-400	0.28	/	0.78	0	0.28
FNC-500	1.46	0.27	0.36	/	1.04
NC-600	/	/	0.49	0.42	0.38

Table S3. BET and pore size distribution of NC-400, FNC-500 and NC-600.

Samples	$S_{\text{BET}}/\text{m}^2\cdot\text{g}^{-1}$	$V_{\text{total}}/\text{cm}^3\cdot\text{g}^{-1}$	$V_{\text{meso/macro}}/\text{cm}^3\cdot\text{g}^{-1}$	$V_{\text{micro}}/\text{cm}^3\cdot\text{g}^{-1}$	D_{avg}/nm
NC-400	2281	1.076	0.5264	0.5496	2.204
FNC-500	2316	1.345	0.7952	0.5498	2.827
NC-600	2483	1.465	0.9478	0.5172	2.896

Note: S_{BET} : the specific surface area; V_{total} : the total pore volume; D_{avg} : average pore width; $V_{\text{meso/macro}}$: the volume of meso/macropores (2–300 nm); V_{micro} : the volume of micropores (≤ 2 nm); S_{BET} and pore size distribution of samples are calculated by using the Brunauer-Emmett-Teller (BET) equation and the Barrett-Joyner-Halenda (BJH) method, respectively.

Part S4 Study of formation mechanism of porous Fe-N-C materials

Sample treatment

The oily sludge was dried at 80 °C for 24 h (this sample was labelled: “OS-dry”). Then three equal parts of the OS-dry (3 g) were mixed with NaCl to obtain oily sludge to salt ratio by mass: 1: 8, and the mixtures was carbonized under a nitrogen atmosphere by heating at 400, 500 and 600 °C for 2 h with a ramp rate of 5 °C·min⁻¹, named as OS-400, OS-500, OS-600, respectively. In order to study the effect of sodium chloride for structure evolution upon heating, sample was heated under the same situation as OS-500 without adding NaCl, defined as No-NaCl-OS-500.

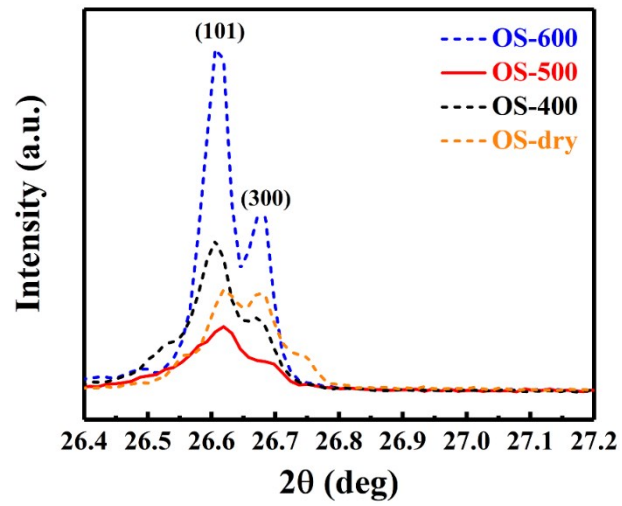


Figure S10. Partial enlarged view of Figure 3b.

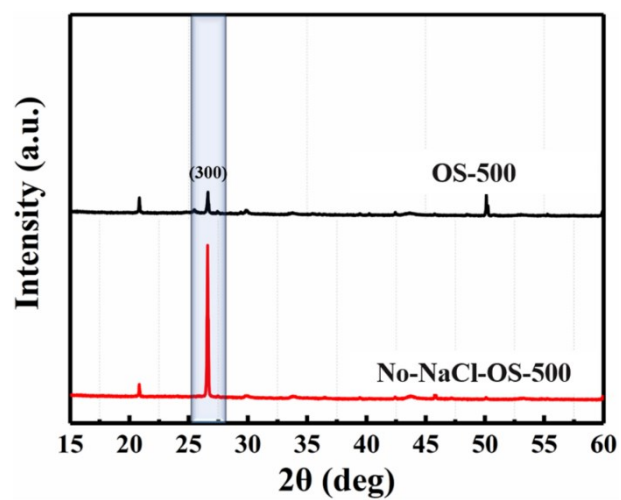


Figure S11. XRD of OS-500 and No-NaCl-OS-500 in presence (dark) and absence (red) of NaCl, respectively.

Part S5 Electrochemical performance of porous Fe-N-C materials

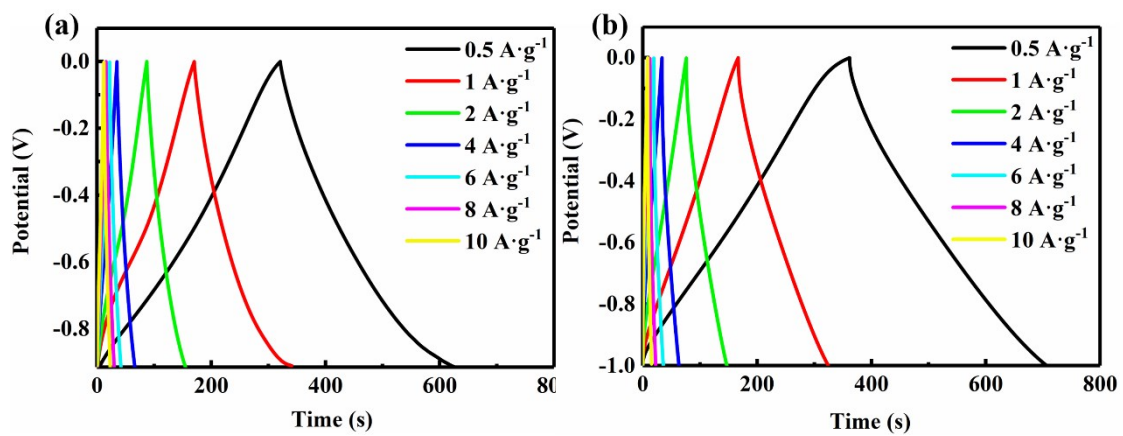


Figure S12. GCD curves of NC-400 (a) and NC-600 (b), respectively.

Table S4. Fitted parameters of some elements in the equivalent circuit.

Sample	R_s (Ω)	R_{ct} (Ω)
NC-400	0.56	1.48
FNC-500	0.58	0.12
NC-600	0.63	0.38

Table S5 Comparison of electrochemical performance of carbon materials from the industrial solid waste with FNC-500.

Carbon Precursor	Activation method	SSA (m²·g⁻¹)	Gravimetric capacitance (F·g⁻¹)	Energy density (Wh·kg⁻¹)	Power density (W·kg⁻¹)	Measurement condition	Ref
Biomass Refinery Wastes	KOH+CO ₂	862	370.0	2.5	180.0	6M KOH 0.5 A·g ⁻¹	1
Oily sludge	HF+KOH	2561	348.1	7.2	100.0	0.5 A·g ⁻¹	2
hydrolysis residue	/	819	141.6	11.7	90.0	1M Na ₂ SO ₄ 0.2 A·g ⁻¹	3
coal tar pitch	KOH + γ -Fe ₂ O ₃	1330	194.0	20.0	120.0	6 M KOH	4
Sugar Industry Spent Wash Waste	hot air+ZnCl ₂	730-900	120.0	16.0	248.0	6 M KOH 1 A·g ⁻¹	5
waste dyed silk fabrics	KOH	30	305.0	10.7	160.7	1M Na ₂ SO ₄ 2 mV·s ⁻¹	6

industrial mill scale waste	HCl	10	92.0	4.0	80.0	0.5 M Na ₂ SO ₃ 5 mV·s ⁻¹	7
tobacco rods	KOH	2115	286.6	31.3	521.0	6 M KOH 0.5 A·g ⁻¹	8
hemp	KOH	2287	142.0	60.0	800.0	6 M KOH 10 A·g ⁻¹	9
bagasse wastes	KOH	3396	320.0	20.0	182.0	6 M KOH 0.5 A·g ⁻¹	10
oily waste sludge	KOH	2316	286.3	33.5	606.1	6 M KOH 0.5 A·g ⁻¹	This work

References

- 1 N. F. He, S. Y. Yoo, J. J. Meng, O. Yildiz, P. D. Bradford, S. Park, W Gao, Engineering biorefinery residues from loblolly pine for supercapacitor applications, *Carbon*, 2017, **120**, 304-312.
- 2 X. Li, J. Zhao, Z. S. Cai, F. Y. Ge. Hierarchical porous carbon from hazardous waste oily sludge for all-solid-state flexible supercapacitor, *Electrochimica Acta*, 2017, **240**, 43-52.
- 3 P. Y. Li, H. Y. Xie, Y. L. Liu, J. Wang, Y. Xie, W. R. Hu, T. H. Xie, Y. B. Wang, Y. K. Zhang, Molten salt and air induced nitrogen-containing graphitic hierarchical porous biocarbon nanosheets derived from kitchen waste hydrolysis residue for energy storage, *J. Power Sources*, 2019, **439**, 227096.
- 4 X. J. He, N. Zhao, J. S. Qiu, N. Xiao, M. X. Yu, C. Yu, X. Y. Zhang, M. D. Zheng, Synthesis of hierarchical porous carbons for supercapacitors from coal tar pitch with nano-Fe₂O₃ as template and activation agent coupled with KOH activation, *J. Mater. Chem., A* 2013, **1**, 9440.
- 5 A. Mahto, R. Gupta, K. K. Ghara, D. N. Srivastava, P. D. K. Maiti, P. Z. Rivera, R. Meena, S. K. Nataraj, Development of high-performance supercapacitor electrode derived from sugar industry spent wash waste, *J. Hazard. Mater.*, 2017, **340**, 189-201.
- 6 X. Li, J. Zhao, Z. S. Gai, F. Y. Ge, Free-standing carbon electrode materials with three-dimensional hierarchically porous structure derived from waste dyed silk fabrics, *Mater. Res. Bull.*, 2018, **107**, 355-360.
- 7 C. Fu, S. G. Patrick, Toward low-cost grid scale energy storage: supercapacitors based on up-cycled industrial mill scale waste, *ACS Sustain. Chem. Eng.*, 2015, **3**, 2831-2838.

8 Y. Q. Zhao, M. Lu, P. Y. Tao, Y. J. Zhang, X. T. Gong, Z. Yang, G. Q. Zhang, H. L. Li, Hierarchically porous and heteroatom doped carbon derived from tobacco rods for supercapacitors, *J. Power Sources*, 2016, **307**, 391-400.

9 H. L. Wang, Z. W. Xu, K. Alireza, Z. Li, K. Cui, X. H.; Tan, T. J. Stephenson, C, K. King Ondu, C. M. B. Holt, B. C. Olsen, J. K. Tak, D. Harfield, A. O. Anyia, D. Mitlin, Interconnected carbon nanosheets derived from hemp for ultrafast supercapacitors with high energy, *ACS Nano*, 2013, **7**, 5131-5141.

10 H. B. Feng, H. Hang, H. W. Dong, Y. Xiao, Y. J. Cai, B. F. Lei, Y. L. Liu, M. T. Zheng, Hierarchical structured carbon derived from bagasse wastes: a simple and efficient synthesis route and its improved electrochemical properties for high-performance supercapacitors, *J. Power Sources*, 2016, **302**, 164-173.